Graphical Abstract

Coaxial multi-criteria optimization of a methane steam reforming reactor for effective hydrogen production and thermal management

Marcin Pajak, Grzegorz Brus, Janusz S. Szmyd

Highlights

Coaxial multi-criteria optimization of a methane steam reforming reactor for effective hydrogen production and thermal management

Marcin Pajak, Grzegorz Brus, Janusz S. Szmyd

- Introduction of a novel approach to the macro-patterning concept.
- Sensitivity analysis conducted for the evolutionary algorithm parameters.
- Enhancement of thermal conditions via a modification of the catalyst insert.
- Increase in hydrogen productivity.

Coaxial multi-criteria optimization of a methane steam reforming reactor for effective hydrogen production and thermal management

Marcin Pajak[a,*], Grzegorz Brus[a], Janusz S. Szmyd[a]

[a] *AGH University of Science and Technology, Krakow, Poland*

Abstract

The advancement in environmental awareness is the recent driving factor of the energy industry development. The market sentiments dictate the commercialization of unconventional energy sources. Thus, generation via hydrogen conversion gains popularity. The presented research regards the enhancement of the steam reforming reaction, used for the production of hydrogen via the conversion of hydrocarbons. The reforming process characterizes by a strong endothermic nature. The rapid course of the reaction leads to the creation of temperature gradients of a considerable magnitude. The presented research strives to alleviate the negative consequences of the reaction character. An original strategy by the name of macro-patterning is suggested as a remedy. The presented research proposes an updated concept, predicting the introduction of coaxial segments to the catalytic insert. The segments may consist of catalytic material or metallic foam applied for local suppression of the reaction. The morphology of specific segments may be altered independently, to allow for additional control of the reforming reaction. The objective of the research is to define the optimal segment composition. The optimization process is based on an in-house procedure implementing a genetic algorithm. The acquired results appear to validate the macro-pattering concept. A significant unification of the temperature field is obtained, with a simultaneous increase in hydrogen productivity.

Keywords: hydrogen, evolutionary algorithms, reforming, design optimization

*Corresponding author

Email address: mpajak@agh.edu.pl (Marcin Pajak)

1. Introduction

Hydrogen technologies are one of the promising directions of the clean energy sector development [1]. The research on hydrogen is conducted to provide a reliable alternative to the currently dominant fossil fuel energy sources [2, 3]. Hydrogen might be used as an energy carrier for internal combustion or fuel cells, both resulting in steam being the main product [4, 5]. However, with the application of hydrogen technology, some crucial issues arise. The first issue regards hydrogen acquisition, as it does not occur on Earth in its pure form. The second matter is hydrogen storage, with currently no effective measures of long-term storage [6, 7]. The two most common processes for on-the-spot production of hydrogen are water electrolysis and the reforming of hydrocarbons [8, 9]. Water electrolysis is a process predicting the breaking of chemical bonds between oxygen and hydrogen in particles of water. The current state of the electrolysis development is far from meeting economical requirements [10]. The only reasonable use of water electrolysis is to deplete surplus energy generated from renewable sources during low market demand and short-term storage of hydrogen for further use during increased demand for energy [11]. The second measure for hydrogen production is the reforming reaction [12, 13]. The reforming process is a catalytic reaction used for the conversion of hydrocarbons for the production of hydrogen [14, 15]. The reforming process can be successfully applied to the conversion of biofuels, allowing the reforming process to be considered a renewable hydrogen source [16, 17]. Furthermore, the process can be successfully applied as a measure of carbohydrate-based waste gases or plastic recycling, establishing it as a prominent for hydrogen generation [18, 19]. The reforming technology brings a series of issues regarding the thermal conditions occurring inside the reactor. The strong endothermic nature of the process results in the occurrence of thermal stresses and may lead to a shortening of the reactor's lifespan [20]. The presented research aims to reduce the drawbacks of the process, by enhancement of the thermal conditions. The majority of researchers focused on the parametric study and optimization of the reaction conditions, resulting in improvements only to a certain extent [21, 22]. Further development of the process is pursued by the introduction of new materials and design concepts, including new catalyst structures [23, 24], the introduction of new kinds of catalyst supports [25], or by rethinking the

design of the reactor itself [26, 27, 28]. A captivating opportunity is described in a work by Palma et al. [29], who introduced a structured catalyst for the intensification of the reforming reaction. The research confirms the improvement of the reaction rate, resulting from the enhancement of the axial and radial temperature distribution. The research reported by Yun et al. [30] focuses on the enhancement of heat transfer, by modification of the design, to acquire a maximized heat transfer area. The proper handling of heat in the reforming process is confirmed to enhance the overall process conduction [31]. Furthermore, a rapid temperature decay at the upstream region of the reactor results in thermal stresses forming in the reactor. Thus, leading to its uneven degradation and reduction of the unit's lifetime [32]. A unification of the temperature distribution may not only improve the conditions but also achieve easier control of the process [33]. The presented research aims to alleviate the negative consequences of the strong endothermic character of the process, via the introduction of radial division of the catalytic insert. The concept originates from the approach proposed by Settar et al. [34]. The research predicted an introduction of macro-patterned active surfaces with an introduction of metallic foam matrices, focusing on providing advantageous thermal conditions for the reaction [35, 36]. The presented research extends the concept to fill the whole reactor's volume with a catalytic composite of nickel and yttria-stabilized zirconia (Ni/YSZ), to maximize the reaction region in the reactor. Further, the reforming unit is divided into segments in the radial direction, instead of the longitudinal division [37]. Non-catalytic metallic foam is used as a substitute for parts of the catalyst, to adjust the intensity of the reaction proceeding, leading to the unification of the thermal field inside the reactor. To define the optimal alignment of the catalyst, an evolutionary algorithm is coupled with an in-house reforming simulation [38]. The presented analysis includes:

- Investigation of the macro-patterning concept applicability with the introduction of the catalytic insert radial division.
- Introduction of two separate principles for the configuration of the segments.
- Comprehensive sensitivity analysis to define the finest performing set of the evolutionary algorithm parameters.
- Analysis of the results robustness, via measuring the hydrogen productivity of specimens defined by the specific algorithms.

2. Mathematical model

Basing on the presented literature review, a relevant mathematical model is composed. The model encapsulates all of the relevant transport phenomena, occurring during the reforming process in a micro-scale reactor. The reforming unit consists of steel cylindrical pipe, which is filled with catalytic material and steel foam. Both of these materials are considered to be porous. The fine powder mixture of nickel and yttria-stabilized zirconia (Ni/YSZ) is used as the catalyst. The arrangement of the porous materials inside the tube is crucial. The whole reactor is divided into separate segments in the longitudinal and radial directions. The segments are randomly chosen to be filled with Ni/YSZ or steel foam. Methane (CH_4) is used as a fuel for the reaction and is supplied with a specified quantity of steam (H_2O) and carbon dioxide (CO_2) at the inlet, fulfilling the steam-to-carbon (SC) or carbon-to-carbon (CC) ratios. SC represents the ratio of steam to methane fed to the reactor, while CC describes the ratio of carbon monoxide to methane at the reactor's inlet. The analyzed model is steady. The basis of the model originates from the research conducted by Xu and Froment. [39]. The mathematical description of the reaction presented by the authors is one of the most fundamental papers in the field of numerical analysis of the reforming process. The accuracy of the approach presented by the authors is proven among works of many different researchers [40, 41, 27, 42] Thus, it has been chosen as a starting point for the development of the model applied in the presented research. The complex character of the reforming process' physics has a consequence in a significant computational cost. Proper formulation of the problem analysis is essential to optimize the computational cost of the reforming process' simulation.

2.1. Reactor's geometry

Depending on the type of fuel used, the moderation of the temperature distribution may require different configurations of the catalyst segments. With a modification in fuel composition, the process' thermodynamical conditions change. Following, to conduct the reforming reaction under optimal conditions, a replacement of the catalyst insert may be required. The reactor has to be designed accordingly, to allow an accessible modification of the insert in a real-life scenario. Thus, the computational domain has to be prepared in a way fulfilling the given assumptions. Furthermore, the described reforming process simulation is meant to be coupled with a genetic

algorithm. Therefore, the limitation of the computational time is a crucial aspect of the presented analysis as well. The reactor's geometry complexity has to be restricted, allowing for a meaningful limitation of the calculation time [43]. Following, the reactor analyzed in the presented research is assumed to be a plug-flow reactor, maintaining axial symmetry throughout its whole volume. The reactor consists of a straight, cylindrical pipe, allowing for an accessible replacement of the catalyst insert when required. Furthermore, the described approach allows for a significant reduction of the number of systems of equations necessary for composing a correct solution for the mathematical relations introduced to the model [44]. The reformer's body is assumed to be filled with porous media. Due to the listed assumptions, the method of volume averaging is used to compose the governing equations, properly describing the transport and heat transfer of the fluids taking part in the process. The method allows for a relevant description of the fluid behavior and its interaction with the porous structure of the reformer's porous catalyst insert [45, 46]. The main objective of the dissertation is to optimize the temperature distribution inside the reactor, enhance the process effectiveness, and alleviate the negative consequences of the thermal stresses occurring during the described process [32, 29]. The introduced macro-patterning strategy predicts modification of the catalyst insert's morphology and its partial substitution with a non-catalytic material. Substitution of the catalyst material serves to enhance the heat transfer inside the reactor [37]. According to the current state of the art, metallic foams appear a promising solution for the indicated issues [47]. An appropriate alloy may certainly fulfill all of the requirements regarding the foam's catalytic activity, diffusional, and thermal properties [48, 49]. The reforming process characterizes itself with values of the temperature established at levels differentiating from approximately 500° C to 1100° C, simultaneously vastly reducing the number of possible choices of the metallic foam alloys [50, 51]. The selection is further narrowed by a requirement of reaction suppression while entering a non-catalytic zone of the insert. Therefore, the chosen material has to withstand the adverse thermal conditions, at relatively high temperatures, and demonstrate inferior catalytic activity during the reforming process. According to the literature, stainless steel foam could be a suitable choice. The stainless steel foam provides appropriate thermal properties at the described conditions [52, 53]. The catalytic activity reported for the stainless steel is several orders of magnitude lower when compared with the conventional catalyst materials, frequently used for the hydrogen

production on the way of the reforming process [54, 55, 56, 57]. To provide a relevant measure for altering the temperature distribution inside the reactor, the catalyst insert is divided into segments. Each segment may consist of a catalyst or a non-catalytic material, with their morphological parameters individually assigned. The insert's segmentation is carried out according to three separate strategies. The first strategy predicts division in the longitudinal direction, resulting in cylinders placed sequentially along the reactor's axis (Fig. 1 a)). The second strategy predicts the catalyst insert to consist of concentric rings, as a result of the insert's division along the reactor's radius (Fig. 1 b)). The third strategy combines both of the aforementioned approaches (Fig. 1 c)). The applied types of catalyst segmentation are illustrated in Fig. 1. The proposed configurations of the catalyst insert provide a convenient way of replacing whole or even parts of the catalyst setup when required. Furthermore, the design containing exclusively simple geometrical shapes, allows maintaining an insignificant computational complexity of the domain [43].

2.2. Computational Domain

The reactor's axial symmetry implies the application of the symmetry boundary condition at the symmetry axis [44]. The mathematical model can be simplified, relying on the assumption that transport and chemical phenomena occur in an identical manner around the reactor's axis. Therefore, the angular dimension may be neglected. To complete the essential assumptions for a proper analysis of the problem, the no-slip boundary condition is applied to the reactor's wall. A preview of the boundary conditions is presented in Fig. 2.

The assumption of axial symmetry allows the computational domain to be limited to two dimensions only. Thus, constraining the domain by a rectangle contained by the reactor's axis and its radius, being a two-dimensional cross-section of the reformer itself [32, 37]. Following, the prepared simulation is considered a quasi-three-dimensional analysis. The computational domain restricted for the needs of the presented analysis is illustrated in Fig. 3.

The computational domain in Fig. 3 is indicated with the dashed blue line. The overall computation is based on the equations describing the chemical reactions and transport processes occurring inside the indicated two-dimensional region. The indicated region combines the insert's cross-section and the reactor's wall fragment.

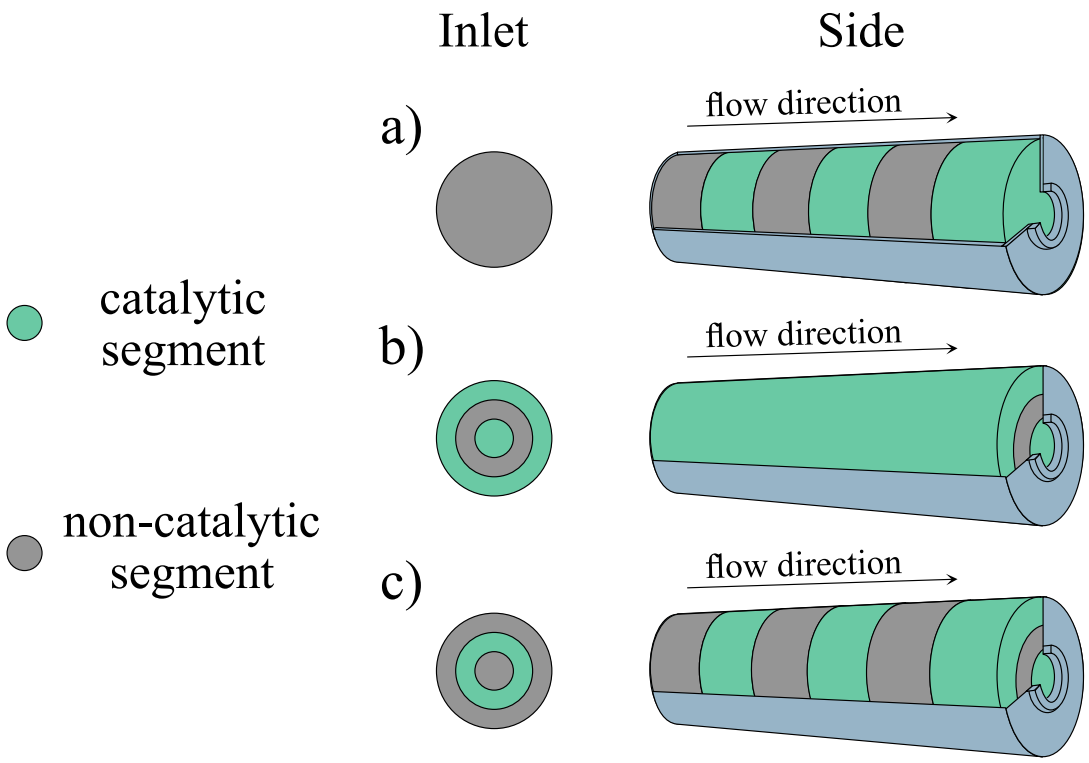

Figure 1: The investigated macro-patterinig designs: a) catalyst insert's division in the longitudinal direction, b) catalyst insert's division in the radial direction, c) both strategies combined

2.3. Chemical Reactions Model

The inclusion of a mathematical representation of the chemical reactions is required for the definition of a proper model. The process is assumed to be dominated by three reactions, as reported in literature [39, 58, 33]. The reactions are steam reforming of methane (MSR) (Eq. (1)), dry reforming of methane (DRY) (Eq. (2)), and water-gas shift reaction (WGS) (Eq. (3)) [59]. The stoichiometric equations for the reactions are presented below:

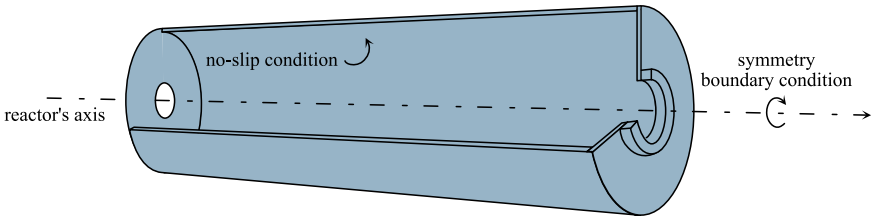

Figure 2: Boundary conditions related to the reactor's geometry

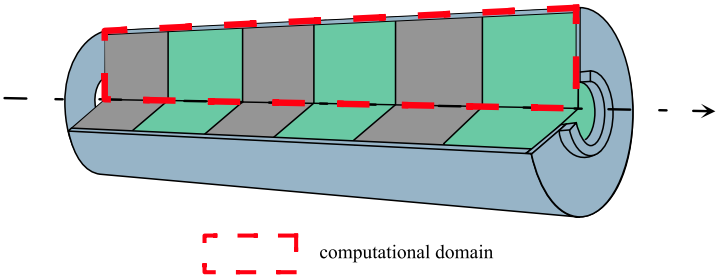

Figure 3: Computational domain

$$\mathrm{CH_4 + H_2O \rightarrow 3H_2 + CO},$$
$$\Delta H_{\mathrm{MSR}} = 206.1 \frac{\mathrm{kJ}}{\mathrm{mol}}, \quad (1)$$

$$\mathrm{CH_4 + CO_2 \rightleftharpoons 2H_2 + 2CO},$$
$$\Delta H_{\mathrm{DRY}} = 247 \frac{\mathrm{kJ}}{\mathrm{mol}}, \quad (2)$$

$$\mathrm{CO + H_2O \rightleftharpoons H_2 + CO_2},$$
$$\Delta H_{\mathrm{WGS}} = -41.15 \frac{\mathrm{kJ}}{\mathrm{mol}}. \quad (3)$$

The reformer is supplied with a mixture of H_2, CO_2, and CH_4. The exact composition of the inlet gases is determined by two parameters. The first is the steam-to-carbon ratio (SC), defining the ratio of steam to methane at the reactor's inlet. The second parameter is the carbon-to-carbon ratio (CC), equal to the ratio of carbon dioxide to methane at the inlet. The process conditions are remarkably influenced by the SC and CC values, as the reactions' rates depend directly on the composition of the inlet gases [60]. A proper setting of the values of the ratios is crucial for the prevention of the carbon deposition phenomenon [61]. Adverse process conditions can result in carbon particles precipitating on the catalyst surface. Thus, reducing the active surface of the catalyst, leading to its poisoning. A proper setting of the ratios and the process' temperature are proven to have the most significant influence on the alleviation of the poisoning hazard [62]. The enthalpy changes ΔH are taken from literature [37, 63]. To allow the inclusion of the reactions into the model, knowledge of their rates is essential. According to the research conducted by Brus et al. [41], the effective rate of MSR and DRY reactions can be expressed with a common equation:

$$R_{\text{eff}} = \dot{w}_{\text{cat}} A_{\text{MSR}} \exp\left(-\frac{E_{\text{a}}}{\overline{R}T}\right) p_{\text{CH}_4}^{\alpha} \left(p_{\text{H}_2\text{O}} + p_{\text{CO}_2}\right)^{\beta}. \tag{4}$$

The individual reaction rates for the MSR and DRY reactions can be distinguished as follows:

$$R_{\text{MSR}} = R_{\text{eff}} \frac{p_{\text{H}_2\text{O}}}{p_{\text{CO}_2} + p_{\text{H}_2\text{O}}}, \tag{5}$$

$$R_{\text{DRY}} = R_{\text{eff}} \frac{p_{\text{CO}_2}}{p_{\text{CO}_2} + p_{\text{H}_2\text{O}}}. \tag{6}$$

The reforming reaction is reported to occur rather slowly [64]. However, the WGS reaction has a more unpredictable nature [65]. Thus, the preparation of a formula, returning proper values regardless of the process conditions, is not feasible. According to Ahmed and Föger, the WGS reaction can be assumed to maintain equilibrium under specific conditions [66]. The equilibrium assumption has been successfully applied in other numerical analyses [67, 68, 69]. The assumption also meets a good agreement between the calculations and the experimental data [70, 71, 72]. Taking into account the

provided literature review, the WGS reaction is assumed to be in the equilibrium state in the presented analysis. The boundary conditions applied in the presented research, described in Section **??**, are designed to satisfy the equilibrium assumption. Following the statements, CO, CO_2, H_2 and H_2O have to satisfy the equilibrium equation, expressed by the following formula:

$$K_{\mathrm{WGS}} = \frac{k^{+}_{\mathrm{WGS}}}{k^{-}_{\mathrm{WGS}}} = \frac{p_{\mathrm{CO_2}} p_{\mathrm{H_2}}}{p_{\mathrm{CO}} p_{\mathrm{H_2O}}} = \exp\left(-\frac{\Delta G^{0}_{\mathrm{WGS}}}{\overline{R}T}\right). \tag{7}$$

The WGS reaction rate can be further expressed using Eq. (8):

$$R_{\mathrm{WGS}} = k^{+}_{\mathrm{WGS}} p_{\mathrm{CO}} p_{\mathrm{H_2O}} + k^{-}_{\mathrm{WGS}} p_{\mathrm{H_2}} p_{\mathrm{CO_2}}. \tag{8}$$

The value of R_{WGS1} can be acquired through the analysis of the reforming process stoichiometry and balancing the chemical species. Following, the methane conversion rate xcr and carbon monoxide conversion rate ycr can be specified:

$$xcr = 1 - \frac{n^{\mathrm{inlet}}_{\mathrm{CH_4}} - R_{\mathrm{MSR}} V}{n^{\mathrm{inlet}}_{\mathrm{CH_4}}}, \tag{9}$$

$$ycr = \frac{K_{\mathrm{WGS}} + 3xcr - \sqrt{\chi - \omega}}{2(K_{\mathrm{WGS}} - 1)}, \tag{10}$$

where:

$$\chi = (K_{\mathrm{WGS}} SC + 3xcr)^2, \tag{11}$$

$$\omega = 4K_{\mathrm{WGS}} xcr(K_{\mathrm{WGS}} - 1)(SC - xcr). \tag{12}$$

Further balancing the reaction's stoichiometry allows for the calculation of the partial pressures included in Eq. (7), leading to the relation describing the WGS reactions' rate (Eq. (13)) [41].

$$R_{\mathrm{WGS}} = \frac{n^{\mathrm{outlet}}_{\mathrm{CH_4}}}{V} = \frac{n^{\mathrm{inlet}}_{\mathrm{CH_4}} \cdot xcr}{V} ycr. \tag{13}$$

After connecting Eq. (9) with Eq. (13) and applying simple mathematical transformations, a final expression for the WGS reaction's rate is formed:

$$R_{\mathrm{WGS}} = R_{\mathrm{MSR}} ycr. \tag{14}$$

The mass consumption and production rates of the reforming process reactions (Eqs. (1) - (3)), are summarized in the Table 1. The values are further applied to the mass transfer equation (Eq. (19)), as a part of its source terms. The heat generation rates by the described reactions are calculated depending on the rates of the reactions (Eqs. (5), (6), (14)) and the values of enthalpy change ΔH [39, 41]. The heat generation rates are given below:

$$Q_{\mathrm{MSR}} = -\Delta H_{\mathrm{MSR}} R_{\mathrm{MSR}}, \tag{15}$$

$$Q_{\mathrm{DRY}} = -\Delta H_{\mathrm{DRY}} R_{\mathrm{DRY}}, \tag{16}$$

$$Q_{\mathrm{WGS}} = -\Delta H_{\mathrm{WGS}} R_{\mathrm{WGS}}. \tag{17}$$

Table 1: Mass sources/sinks

species	mass generation MSR	mass generation WGS	mass generation DRY	summarized generation
H_2	$3R_{\mathrm{MSR}}M_{\mathrm{H_2}}$	$R_{\mathrm{WGS}}M_{\mathrm{H_2}}$	$2R_{\mathrm{DRY}}M_{\mathrm{H_2}}$	$3R_{\mathrm{MSR}}M_{\mathrm{H_2}} + R_{\mathrm{WGS}}M_{\mathrm{H_2}} + 2R_{\mathrm{DRY}}M_{\mathrm{H_2}}$
CO	$R_{\mathrm{MSR}}M_{\mathrm{CO}}$	$-R_{\mathrm{WGS}}M_{\mathrm{CO}}$	$2R_{\mathrm{DRY}}M_{\mathrm{CO}}$	$R_{\mathrm{MSR}}M_{\mathrm{CO}} - R_{\mathrm{WGS}}M_{\mathrm{CO}} + 2R_{\mathrm{DRY}}M_{\mathrm{CO}}$
CO_2	0	$R_{\mathrm{WGS}}M_{\mathrm{CO_2}}$	$-R_{\mathrm{DRY}}M_{\mathrm{CO_2}}$	$R_{\mathrm{WGS}}M_{\mathrm{CO_2}} -2R_{\mathrm{DRY}}M_{\mathrm{H_2}}$
CH_4	$-R_{\mathrm{MSR}}M_{\mathrm{CH_4}}$	0	$-R_{\mathrm{DRY}}M_{\mathrm{H_2}}$	$-R_{\mathrm{MSR}}M_{\mathrm{CH_4}} -R_{\mathrm{DRY}}M_{\mathrm{H_2}}$
H_2O	$-R_{\mathrm{MSR}}M_{\mathrm{H_2O}}$	$-R_{\mathrm{WGS}}M_{\mathrm{H_2O}}$	0	$-R_{\mathrm{MSR}}M_{\mathrm{H_2O}} -R_{\mathrm{WGS}}M_{\mathrm{H_2O}}$

2.4. Heat and Mass Transfer Model

The fundamental transport equations are incorporated into the mathematical model. Considering the computational domain defined for the needs of the analysis, the equations are implemented for two dimensions. Therefore, the model's equations are solved along the axis and radius of the reactor's geometry. The volume-averaging method was chosen for the derivation of the governing equations implemented in the model used for this analysis. The process parameters are locally averaged for each representative volume and included in the mathematical formulas [73]. Values of continuity (Eq. (18)), mass transfer (Eq. (19)), momentum (Eqs. (21) and (22)) and energy equations (Eq. (27)) characterize the transport phenomena occurring during the reforming process. The equations are derived for the laminar flow. The analyzed fluids are considered to be Newtonian and incompressible. Thus, the continuity equation takes the following form [74, 75]:

$$\frac{\partial\left(\rho_0 U_x\right)}{\partial x}+\frac{1}{r}\frac{\partial\left(r\rho_0 U_r\right)}{\partial r}=0, \tag{18}$$

The species conservation is calculated using molar fractions of species taking part in the reaction (Equation (19)). The formulated equation is derived from Fick's law of diffusion [33]. The mass sources and sinks S_j depend on the MSR, DRY, and WGS rates and molar masses of the species taking part in the reaction [76, 20]. The exact equations defining the values of S_j are described in Table 1.

$$\begin{aligned}\rho_0\left(U_x\frac{\partial Y_j}{\partial x}+U_r\frac{\partial Y_j}{\partial r}\right)=&\frac{\partial}{\partial x}\left(\rho_0 D_{j,\mathrm{eff}}\frac{\partial Y_j}{\partial x}\right)\\&+\frac{1}{r}\frac{\partial}{\partial r}\left(r\rho_0 D_{j,\mathrm{eff}}\frac{\partial Y_j}{\partial r}\right)+S_j.\end{aligned} \tag{19}$$

The effective mass diffusivity of species $D_{j\mathrm{eff}}$ was calculated using the equation explained below (Eq. (20)) [77]:

$$D_{j,\mathrm{eff}}=(1-\sqrt{1-\varepsilon_0})D_j. \tag{20}$$

The diffusion of substance j in the gas mixture D_j is computed using Fuller's method and Blanc's law. The gases' properties are taken from the literature [78]. The values assumed for the flow model describe the local phase

average of the gas control volume. The momentum conservation depends directly on the insert's morphology. The materials composing the insert are considered porous. Therefore, parameters describing the material structure have to be included in the equations. The parameters are porosity ε_0, permeability K_p, and inertial coefficient c_{ine} [38]. A separate momentum equation is formulated for each of the computational domain dimensions (Eqs. (21) and (22)).

$$\frac{\rho_0}{\varepsilon_0^2}\left(U_x\frac{\partial U_x}{\partial x}+U_r\frac{\partial U_x}{\partial r}\right)=-\frac{\partial P}{\partial x}+\frac{\mu}{\varepsilon_0}\left[\frac{\partial^2 U_x}{\partial x^2}+\frac{1}{r}\frac{\partial}{\partial r}\left(r\frac{\partial U_x}{\partial r}\right)\right] - \frac{\mu}{K_{\text{p}}}U_x-\frac{\rho_0 c_{\text{ine}}}{\sqrt{K_{\text{p}}}}U_x\sqrt{U_x^2+U_r^2}, \tag{21}$$

$$\frac{\rho_0}{\varepsilon_0^2}\left(U_x\frac{\partial U_r}{\partial x}+U_r\frac{\partial U_r}{\partial r}\right)=-\frac{\partial P}{\partial r}+\frac{\mu}{\varepsilon_0}\left[\frac{\partial^2 U_r}{\partial x^2}+\frac{1}{r}\frac{\partial}{\partial r}\left(r\frac{\partial U_r}{\partial r}\right)-\frac{U_r}{r^2}\right] - \frac{\mu}{K_{\text{p}}}U_r-\frac{\rho_0 c_{\text{ine}}}{\sqrt{K_{\text{p}}}}U_r\sqrt{U_x^2+U_r^2}. \tag{22}$$

The permeability K_{p} of the specific segment is calculated using (23), basing on the information about its porosity ε_0 [79]:

$$K_{\text{p}}=\frac{\varepsilon_0(1-(1-\varepsilon_0)^{1/3})}{36((1-\varepsilon_0)^{1/3}-(1-\varepsilon_0))}d_{\text{p}}^2, \tag{23}$$

where d_{p} stands for an average pore diameter. The inertial coefficient c_{ine} was calculated using [80]:

$$c_{\text{ine}}=0.0095 g_{\text{s}}^{-0.8}\sqrt{\frac{\varepsilon_0}{3(\tau-1)}}\left(1.18\sqrt{\frac{(1-\varepsilon_0)}{3\pi}}\frac{1}{g_{\text{s}}}\right)^{-1}, \tag{24}$$

where tortousity τ and and shape function g_{s} are expressed with following equations [79, 80]:

$$\tau=\frac{\varepsilon_0}{1-(1-\varepsilon_0)^{1/3}}, \tag{25}$$

$$g_{\text{s}}=1-\exp\left(-\frac{1-\varepsilon_0}{0.04}\right). \tag{26}$$

The energy conservation equation (Eq. (27)) describes the process of heat transfer during the reaction. The equation includes local thermal conditions, the materials' parameters, and the heat sources calculated using Eqs. (15) - (17).

$$\rho_0 C_p \left(U_x \frac{\partial T_{\text{loc}}}{\partial x} + U_r \frac{\partial T_{\text{loc}}}{\partial r} \right) = \frac{\partial}{\partial x} \left(\lambda_{\text{eff}} \frac{\partial T_{\text{loc}}}{\partial x} \right) + \frac{1}{r} \frac{\partial}{\partial r} \left(r \lambda_{\text{eff}} \frac{\partial T_{\text{loc}}}{\partial r} \right) + Q_{\text{s}}. \quad (27)$$

The heat transfer model applied in the presented research requires effective thermal conductivity λ_{eff} (Eq. (28)) to be characterized. The reactor's insert may contain segments consisting of metallic foam. Thus, defining a proper relation describing the λ_{eff} of the material is essential [80, 81]. The model chosen for calculating the value of the λ_{eff} was proposed by Boomsma and Poulikakos [82]. The authors have explained the process of thermal conduction inside a metal foam. The research had further corrections applied by Dai et al. [81] and the outcome relation allows for the derivation of equations describing the thermal conductivity of metallic foams. According to the literature review, an adequate model including the morphology of metallic foams is prepared [83].

$$\lambda_{\text{eff}} = \frac{\sqrt{2} l}{2(R_{\text{A}} + R_{\text{B}} + R_{\text{C}} + R_{\text{D}})}, \quad (28)$$

where R_{A} - R_{D} stand for the thermal resistances of the porous media cell subsections and can be calculated as follows [81]:

$$R_{\text{A}} = \frac{4dl}{(2e^2 + d\pi(1-e))\lambda_{\text{solid}}} + \frac{4dl}{(4 - (2e^2 + d\pi(1-e)))\lambda_{\text{mix}}}, \quad (29)$$

$$R_{\text{B}} = \frac{(e - 2d)l}{e^2 \lambda_{\text{solid}} + (2 - e^2)\lambda_{\text{mix}}}, \quad (30)$$

$$R_{\text{C}} = \frac{(\sqrt{2} - 2e)l}{\pi d^2 \lambda_{\text{solid}} \sqrt{2} + (2 - \pi d^2 \sqrt{2})\lambda_{\text{mix}}}, \quad (31)$$

$$R_{\mathrm{D}} = \frac{2el}{e^2\lambda_{\mathrm{solid}} + (4-e^2)\lambda_{\mathrm{mix}}}. \tag{32}$$

The formulas used for calculating R_{A}, R_{D}, R_{C}, and R_{D} require knowledge of the value of the foam ligament radius d (Eq. (33)). The d value can be calculated using the following equation [83]:

$$d = \sqrt{\frac{\sqrt{2}(2 - 2\varepsilon_0 - \frac{3\sqrt{2}}{4}e^3}{\pi(3 - e - 4e\sqrt{2})}}. \tag{33}$$

3. Numerical model

4. Numerical analysis

5. Conclusions

References

[1] U. Y. Qazi, Future of hydrogen as an alternative fuel for next-generation industrial applications; challenges and expected opportunities, Energies 15 (2022). URL: https://www.mdpi.com/1996-1073/15/13/4741. doi:10.3390/en15134741.

[2] C. Zou, Q. Zhao, G. Zhang, B. Xiong, Energy revolution: From a fossil energy era to a new energy era, Natural Gas Industry B 3 (2016) 1–11. doi:https://doi.org/10.1016/j.ngib.2016.02.001.

[3] G. Liobikienė, R. Dagiliūtė, Do positive aspects of renewable energy contribute to the willingness to pay more for green energy?, Energy 231 (2021) 120817. doi:https://doi.org/10.1016/j.energy.2021.120817.

[4] H. Xu, J. Ma, P. Tan, B. Chen, Z. Wu, Y. Zhang, H. Wang, J. Xuan, M. Ni, Towards online optimisation of solid oxide fuel cell performance: Combining deep learning with multi-physics simulation, Energy and AI 1 (2020) 100003. URL: https://www.sciencedirect.com/science/article/pii/S2666546820300033. doi:https://doi.org/10.1016/j.egyai.2020.100003.

[5] B. Shadidi, G. Najafi, T. Yusaf, A review of hydrogen as a fuel in internal combustion engines, Energies 14 (2021) 6209. doi:10.3390/en14196209.

[6] I. Hassan, H. S. Ramadan, M. A. Saleh, D. Hissel, Hydrogen storage technologies for stationary and mobile applications: Review, analysis and perspectives, Renewable and Sustainable Energy Reviews 149 (2021) 111311. doi:https://doi.org/10.1016/j.rser.2021.111311.

[7] C. Tarhan, M. A. Çil, A study on hydrogen, the clean energy of the future: Hydrogen storage methods, Journal of Energy Storage 40 (2021) 102676. URL: https://www.sciencedirect.com/science/article/pii/S2352152X21004151. doi:https://doi.org/10.1016/j.est.2021.102676.

[8] I. Hassan, H. S. Ramadan, M. A. Saleh, D. Hissel, Hydrogen storage technologies for stationary and mobile applications: Review, analysis and perspectives, Renewable and Sustainable Energy Reviews 149 (2021) 111311.

[9] M. T. Azizan, A. Aqsha, M. Ameen, A. Syuhada, H. Klaus, S. Z. Abidin, F. Sher, Catalytic reforming of oxygenated hydrocarbons for the hydrogen production: an outlook, Biomass Conversion and Biorefinery (2020) 1–24. doi:10.1007/s13399-020-01081-6.

[10] R. Yukesh Kannah, S. Kavitha, Preethi, O. Parthiba Karthikeyan, G. Kumar, N. V. Dai-Viet, J. Rajesh Banu, Techno-economic assessment of various hydrogen production methods – a review, Bioresource Technology 319 (2021) 124175. URL: https://www.sciencedirect.com/science/article/pii/S0960852420314498. doi:https://doi.org/10.1016/j.biortech.2020.124175.

[11] J. Chi, H. Yu, Water electrolysis based on renewable energy for hydrogen production, Chinese Journal of Catalysis 39 (2018) 390–394. doi:https://doi.org/10.1016/S1872-2067(17)62949-8.

[12] H. Zhang, Z. Sun, Y. H. Hu, Steam reforming of methane: Current states of catalyst design and process upgrading, Renewable and Sustainable Energy Reviews 149 (2021) 111330. URL: https://www.sciencedirect.com/science/article/pii/S136403212100616X. doi:https://doi.org/10.1016/j.rser.2021.111330.

[13] P. Nkulikiyinka, Y. Yan, F. Güleç, V. Manovic, P. T. Clough, Prediction of sorption enhanced steam methane reforming products from machine learning based soft-sensor models, Energy and AI 2 (2020) 100037. URL: https://www.sciencedirect.com/science/article/pii/S2666546820300379. doi:https://doi.org/10.1016/j.egyai.2020.100037.

[14] Z. Taherian, A. Khataee, N. Han, Y. Orooji, Hydrogen production through methane reforming processes using promoted-ni/mesoporous silica: A review, Journal of Industrial and Engineering Chemistry 107 (2022) 20–30. URL: https://www.sciencedirect.com/science/article/pii/S1226086X21006675. doi:https://doi.org/10.1016/j.jiec.2021.12.006.

[15] H. H. Faheem, S. Z. Abbas, A. N. Tabish, L. Fan, F. Maqbool, A review on mathematical modelling of direct internal reforming- solid oxide fuel cells, Journal of Power Sources 520 (2022) 230857. URL: https://www.sciencedirect.com/science/article/pii/S0378775321013446. doi:https://doi.org/10.1016/j.jpowsour.2021.230857.

[16] X. Zhao, B. Joseph, J. Kuhn, S. Ozcan, Biogas reforming to syngas: A review, iScience 23 (2020) 101082. doi:https://doi.org/10.1016/j.isci.2020.101082.

[17] N. Gao, M. H. Milandile, C. Quan, L. Rundong, Critical assessment of plasma tar reforming during biomass gasification: A review on advancement in plasma technology, Journal of Hazardous Materials 421 (2022) 126764. URL: https://www.sciencedirect.com/science/article/pii/S0304389421017295. doi:https://doi.org/10.1016/j.jhazmat.2021.126764.

[18] J. M. Saad, P. T. Williams, Catalytic dry reforming of waste plastics from different waste treatment plants for production of synthesis gases, Waste Management 58 (2016) 214–220. URL: https://www.sciencedirect.com/science/article/pii/S0956053X16305141. doi:https://doi.org/10.1016/j.wasman.2016.09.011.

[19] B. Zhang, Y. Chen, B. Zhang, R. Peng, Q. Lu, W. Yan, B. Yu, F. Liu, J. Zhang, Cyclic performance of coke oven gas - steam reforming with assistance of steel slag derivates for high purity hydrogen production, Renewable Energy 184 (2022) 592–603. URL: https://www.sciencedirect.com/science/article/pii/S0960148121017183. doi:https://doi.org/10.1016/j.renene.2021.11.123.

[20] M. Mozdzierz, G. Brus, A. Sciazko, Y. Komatsu, S. Kimijima, J. S. Szmyd, An attempt to mimimize the temperature gradient along a plug-flow methane/steam reforming reactor by adopting locally controlled heating zones, Journal of Physics: Conference Series **530** (2014) 012040(1)–012040(8).

[21] A. P. Simpson, A. E. Lutz, Exergy analysis of hydrogen production via steam methane reforming, International Journal of Hydrogen Energy 32 (2007) 4811–4820. doi:10.1016/j.ijhydene.2007.08.025.

[22] A. T. Naseri, B. A. Peppley, J. G. Pharoah, A systematic parametric study on the effect of a catalyst coating microstructure on its performance in methane steam reforming, International Journal of Hydrogen Energy 40 (2015) 16086–16095. doi:10.1016/j.ijhydene.2015.10.043.

[23] S. Ali, M. J. Al-Marri, A. G. Abdelmoneim, A. Kumar, M. M. Khader, Catalytic evaluation of nickel nanoparticles in methane steam reforming, International Journal of Hydrogen Energy 41 (2016) 22876–22885. doi:10.1016/j.ijhydene.2016.08.200.

[24] S. T. Kolaczkowski, S. Awdry, T. Smith, D. Thomas, L. Torkuhl, R. Kolvenbach, Potential for metal foams to act as structured catalyst supports in fixed-bed reactors, Catalysis Today 273 (2016) 221–233. doi:10.1016/j.cattod.2016.03.047.

[25] A. K. Yadav, P. D. Vaidya, Renewable hydrogen production by steam reforming of butanol over multiwalled carbon nanotube-supported catalysts, International Journal of Hydrogen Energy 44 (2019) 30014–30023. doi:10.1016/j.ijhydene.2019.09.054.

[26] H. Butcher, C. J. Quenzel, L. Breziner, J. Mettes, B. A. Wilhite, P. Bossard, Design of an annular microchannel reactor (AMR) for hydrogen and/or syngas production via methane steam reforming, International Journal of Hydrogen Energy 39 (2014) 18046–18057. doi:10.1016/j.ijhydene.2014.04.109.

[27] E. Meloni, M. Martino, A Short Review on Ni Based Catalysts and Related Engineering Issues for Methane Steam Reforming, Catalysts 10 (2020) 352. doi:10.3390/catal10030352.

[28] A. Cherif, J.-S. Lee, R. Nebbali, C.-J. Lee, Novel design and multi-objective optimization of autothermal steam methane reformer to enhance hydrogen production and thermal matching, Applied Thermal Engineering 217 (2022) 119140. URL: https://www.sciencedirect.com/science/article/pii/S1359431122010717. doi:https://doi.org/10.1016/j.applthermaleng.2022.119140.

[29] V. Palma, A. Ricca, M. Martino, E. Meloni, Innovative structured catalytic systems for methane steam reforming intensification, Chemical Engineering and Processing: Process Intensification **120** (2017) 207–215.

[30] J. Yun, S. Yu, Transient behavior of 5 kW class shell-and-tube methane steam reformer with intermediate temperature heat source,

International Journal of Heat and Mass Transfer 134 (2019) 600–609. doi:10.1016/j.ijheatmasstransfer.2019.01.078.

[31] A. M. Dubinin, S. E. Shcheklein, V. G. Tuponogov, M. I. Ershov, Mini CHP based on the electrochemical generator and impeded fluidized bed reactor for methane steam reforming, International Journal of Hydrogen Energy 43 (2018) 13543–13549. doi:10.1016/j.ijhydene.2018.05.151.

[32] M. Mozdzierz, G. Brus, A. Sciazko, Y. Komatsu, S. Kimijima, J. S. Szmyd, Towards a Thermal Optimization of a Methane/Steam Reforming Reactor, Flow, Turbulence and Combustion **97** (2016) 171–189.

[33] M. Mozdzierz, M. Chalusiak, S. Kimijima, J. S. Szmyd, G. Brus, An afterburner-powered methane/steam reformer for a solid oxide fuel cells application, Heat and Mass Transfer 54 (2018) 2331–2341. doi:10.1007/s00231-018-2331-5.

[34] A. Settar, R. Nebbali, B. Madani, S. Abboudi, Numerical investigation on the wall-coated steam methane reformer improvement: Effects of catalyst layer patterns and metal foam insertion, International Journal of Hydrogen Energy **42** (2017) 1490–1498.

[35] A. Settar, S. Abboudi, N. Lebaal, Effect of inert metal foam matrices on hydrogen production intensification of methane steam reforming process in wall-coated reformer, International Journal of Hydrogen Energy 43 (2018) 12386–12397. doi:10.1016/j.ijhydene.2018.04.215.

[36] A. Settar, Z. Mansouri, R. Nebbali, Impact of Ni-based catalyst patterning on hydrogen production from MSR : External steam reformer modelling ScienceDirect Impact of Ni-based catalyst patterning on hydrogen production from MSR : External steam reformer modelling, International Journal of Hydrogen Energy 44 (2018) 11346–11354. doi:10.1016/j.ijhydene.2018.09.171.

[37] M. Pajak, M. Mozdzierz, M. Chalusiak, S. Kimijima, J. S. Szmyd, G. Brus, A numerical analysis of heat and mass transfer processes in a macro-patterned methane/steam reforming reactor, International Journal of Hydrogen Energy 43 (2018) 20474–20487. doi:10.1016/j.ijhydene.2018.09.058.

[38] M. Pajak, G. Brus, J. S. Szmyd, Genetic algorithm-based strategy for the steam reformer optimization, International Journal of Hydrogen Energy (2021, In Press). doi:https://doi.org/10.1016/j.ijhydene.2021.10.046.

[39] J. Xu, G. F. Froment, Methane steam reforming: II. Diffusional limitations and reactor simulation, AIChE Journal **35** (1989) 97–103.

[40] Y. Wang, F. Yoshiba, M. Kawase, T. Watanabe, Performance and effective kinetic models of methane steam reforming over ni/ysz anode of planar sofc, International Journal of Hydrogen Energy 34 (2009) 3885–3893. doi:https://doi.org/10.1016/j.ijhydene.2009.02.073.

[41] G. Brus, Y. Komatsu, S. Kimijima, J. S. Szmyd, An analysis of biogas reforming process on Ni/YSZ and Ni/SDC catalysts, International Journal of Thermodynamics 15 (2012) 43–51.

[42] I. Moura, A. Reis, A. Bresciani, R. Alves, Carbon dioxide abatement by integration of methane bi-reforming process with ammonia and urea synthesis, Renewable and Sustainable Energy Reviews 151 (2021) 111619. doi:https://doi.org/10.1016/j.rser.2021.111619.

[43] A. Kaw, E. K. Kalu, D. Nguyen, Numerical Methods with Applications, University of South Florida, Florida, 2011.

[44] S. V. Patankar, Numerical Heat Transfer and Fluid Flow, Hemisphere, Washington, 1980.

[45] S. Whitaker, The Method of Volume Averaging, in: J. Bear (Ed.), Theory and Applications of Transport in Porous Media, Springer, Dordrecht, 1999. doi:10.1007/978-94-017-3389-2.

[46] G. Brus, K. Miyawaki, H. Iwai, M. Saito, H. Yoshida, Tortuosity of an SOFC anode estimated from saturation currents and a mass transport model in comparison with a real micro-structure, Solid State Ionics 265 (2014) 13–21. doi:10.1016/j.ssi.2014.07.002.

[47] K. Boomsma, D. Poulikakos, F. Zwick, Metal foams as compact high performance heat exchangers, Mechanics of Materials 35 (2003) 1161–1176. doi:https://doi.org/10.1016/j.mechmat.2003.02.001.

[48] A. Abaidi, B. Madani, Intensification of hydrogen production from methanol steam reforming by catalyst segmentation and metallic foam insert, International Journal of Hydrogen Energy 46 (2021) 37583–37598. doi:https://doi.org/10.1016/j.ijhydene.2020.12.183.

[49] P. H. Jadhav, N. Gnanasekaran, Optimum design of heat exchanging device for efficient heat absorption using high porosity metal foams, International Communications in Heat and Mass Transfer 126 (2021) 105475. doi:https://doi.org/10.1016/j.icheatmasstransfer.2021.105475.

[50] Y.-S. Seo, A. Shirley, S. T. Kolaczkowski, Evaluation of thermodynamically favourable operating conditions for production of hydrogen in three different reforming technologies, Journal of Power Sources 108 (2002) 213–225. doi:https://doi.org/10.1016/S0378-7753(02)00027-7.

[51] F. Cverna (Ed.), Thermal Properties of Metals, ASM International, Ohio, 2002.

[52] C. Y. Zhao, T. J. Lu, H. P. Hodson, J. D. Jackson, The temperature dependence of effective thermal conductivity of open-celled steel alloy foams, Materials Science and Engineering A 367 (2004) 123–131. doi:10.1016/j.msea.2003.10.241.

[53] B. H. Smith, S. Szyniszewski, J. F. Hajjar, B. W. Schafer, S. R. Arwade, Steel foam for structures: A review of applications, manufacturing and material properties, Journal of Constructional Steel Research 71 (2012) 1–10. doi:10.1016/j.jcsr.2011.10.028.

[54] E. S. Hecht, G. K. Gupta, H. Zhu, A. M. Dean, R. J. Kee, L. Maier, O. Deutschmann, Methane reforming kinetics within a ni–ysz sofc anode support, Applied Catalysis A: General 295 (2005) 40–51. doi:https://doi.org/10.1016/j.apcata.2005.08.003.

[55] G. Jones, J. G. Jakobsen, S. S. Shim, J. Kleis, M. P. Andersson, J. Rossmeisl, F. Abild-Pedersen, T. Bligaard, S. Helveg, B. Hinnemann, J. R. Rostrup-Nielsen, I. Chorkendorff, J. Sehested, J. K. Nørskov, First principles calculations and experimental insight into methane steam reforming over transition metal catalysts, Journal of Catalysis 259 (2008) 147–160. doi:https://doi.org/10.1016/j.jcat.2008.08.003.

[56] A. Simson, E. Waterman, R. Farrauto, M. Castaldi, Kinetic and process study for ethanol reforming using a rh/pt washcoated monolith catalyst, Applied Catalysis B: Environmental 89 (2009) 58–64. doi:https://doi.org/10.1016/j.apcatb.2008.11.031.

[57] P. Wang, L. Jin, H. Hu, CO2 Reforming of Methane over Fe-Modified Ni-Based Catalyst for Syngas Production, Energy Technology 8 (2020) 1–10. doi:10.1002/ente.201900231.

[58] Y. Komatsu, S. Kimijima, J. S. Szmyd, A performance analysis of a solid oxide fuel cell - micro gas turbine hybrid system using biogas, ECS Transactions 25 (2009) 1061–1070. doi:10.1149/1.3205631.

[59] G. Brus, R. Nowak, J. S. Szmyd, Y. Komatsu, S. Kimijima, An Experimental and Theoretical Approach for the Carbon Deposition Problem During Steam Reforming of Model Biogas, Journal of Theoretical and Applied Mechanics **53** (2015) 273–284. doi:10.15632/jtam-pl.53.2.273.

[60] M. Usman, W. Wan Daud, H. F. Abbas, Dry reforming of methane: Influence of process parameters—a review, Renewable and Sustainable Energy Reviews 45 (2015) 710–744. doi:https://doi.org/10.1016/j.rser.2015.02.026.

[61] W. Koncewicz, M. Moździerz, G. Brus, A fast gaussian process-based method to evaluate carbon deposition during hydrocarbons reforming, International Journal of Hydrogen Energy (2021, In Press). doi:https://doi.org/10.1016/j.ijhydene.2021.07.213.

[62] M. Tomiczek, R. Kaczmarczyk, M. Mozdzierz, G. Brus, A numerical analysis of heat and mass transfer during the steam reforming process of ethane, Heat and Mass Transfer **54** (2018) 2305–2314.

[63] A. Mazhar, A. H. Khoja, A. K. Azad, F. Mushtaq, S. R. Naqvi, S. Shakir, M. Hassan, R. Liaquat, M. Anwar, Performance analysis of TiO2-Modified Co/MgAl2O4 Catalyst for Dry Reforming of Methane in a Fixed Bed Reactor for Syngas (H2, CO) Production, Energies 14 (2021) 3347. doi:10.3390/en14113347.

[64] G. Brus, S. Kimijima, J. S. Szmyd, Experimental and numerical analysis of transport phenomena in an internal indirect fuel reforming type Solid

Oxide Fuel Cells using Ni/SDC as a catalyst, Journal of Physics: Conference Series 395 (2012) 012159. doi:10.1088/1742-6596/395/1/012159.

[65] S. Nagata, A. Momma, T. Kato, Y. Kasuga, Numerical analysis of output characteristics of tubular SOFC with internal reformer, Journal of Power Sources **101** (2001) 60–71.

[66] K. Ahmed, K. Föger, Approach to equilibrium of the water-gas shift reaction on a Ni/zirconia anode under SOFC conditions, Journal of Power Sources **103** (2001) 150–153.

[67] T. W. Song, J. L. Sohn, J. H. Kim, T. S. Kim, S. T. Ro, K. Suzuki, Performance analysis of a tubular solid oxide fuel cell/micro gas turbine hybrid power system based on a quasi-two dimensional model, Journal of Power Sources **142** (2005) 30–42. doi:10.1016/j.jpowsour.2004.10.011.

[68] H. Iwai, Y. Yamamoto, M. Saito, H. Yoshida, Numerical simulation of intermediate-temperature direct-internal-reforming planar solid oxide fuel cell, Energy **36** (2011) 2225–2234.

[69] A. Sciazko, Y. Komatsu, G. Brus, S. Kimijima, J. S. Szmyd, A novel approach to improve the mathematical modelling of the internal reforming process for solid oxide fuel cells using the orthogonal least squares method, International Journal of Hydrogen Energy **39** (2014) 16372–16389. doi:10.1016/j.ijhydene.2014.07.130.

[70] G. Brus, Experimental and numerical studies on chemically reacting gas flow in the porous structure of a solid oxide fuel cells internal fuel reformer, International Journal of Hydrogen Energy 37 (2012) 17225–17234.

[71] A. Sciazko, Y. Komatsu, G. Brus, S. Kimijima, J. S. Szmyd, An Application of Generalized Least Squares Method to an Analysis of Methane/Steam Reforming Process on a Ni/YSZ Catalyst, ECS Transactions **57** (2013) 2987–2996. doi:10.1149/05701.2987ecst.

[72] A. Sciazko, Y. Komatsu, G. Brus, S. Kimijima, J. S. Szmyd, A novel approach to the experimental study on methane/steam reforming kinetics using the Orthogonal Least Squares method, Journal of Power Sources **262** (2014) 245–254. doi:10.1016/j.jpowsour.2014.03.097.

[73] R. G. Carbonell, S. Whitaker, Heat and Mass Transfer in Porous Media. In *Fundamentals of Transport Phenomena in Porous Media*. Editors: J. Bear, M. Y. Corapcioglu, Springer, Dordrecht, 1984.

[74] T. Nishino, H. Komori, H. Iwai, K. Suzuki, Development of a comprehensive numerical model for analyzing a tubular-type indirect internal reforming SOFC, 1st International Fuel Cell Science, Engineering and Technology Conference Rochester, New York, USA:521-528, 2003.

[75] T. Nishino, H. Iwai, K. Suzuki, Comprehensive Numerical Modeling and Analysis of a Cell-Based Indirect Internal Reforming Tubular SOFC, Journal of Fuel Cell Science and Technology **3** (2006) 33–44.

[76] W. C. Tan, H. Iwai, M. Kishimoto, G. Brus, J. S. Szmyd, H. Yoshida, Numerical analysis on effect of aspect ratio of planar solid oxide fuel cell fueled with decomposed ammonia, Journal of Power Sources 384 (2018) 367–378. doi:10.1016/j.jpowsour.2018.03.011.

[77] K. Suzuki, H. Iwai, T. Nishino, Electrochemical and thermo-fluid modeling of a tubular solid oxide fuel cell with accompaning indirect internal fuel reforming. In *Transport Phenomena in Fuel Cells*. Editors: B. Sunden, M. Faghri, WIT Press, Southampton, 2005.

[78] B. E. Poling, J. M. Prausnitz, J. P. O'Connell, The Properties of Gases and Liquids, McGraw-Hill, New York, 2001. doi:10.1016/0894-1777(88)90021-0.

[79] X. Yang, T. J. Lu, T. Kim, An analytical model for permeability of isotropic porous media, Physics Letters, Section A: General, Atomic and Solid State Physics 378 (2014) 2308–2311. doi:10.1016/j.physleta.2014.06.002.

[80] A. Bhattacharya, V. V. Calmidi, R. L. Mahajan, Thermophysical properties of high porosity metal foams, International Journal of Heat and Mass Transfer 45 (2002) 1017–1031. doi:10.1016/S0017-9310(01)00220-4.

[81] Z. Dai, K. Nawaz, Y. G. Park, J. Bock, A. M. Jacobi, Correcting and extending the Boomsma-Poulikakos effective thermal conductivity model for three-dimensional, fluid-saturated metal foams, Interna-

tional Communications in Heat and Mass Transfer **37** (2010) 575–580. doi:10.1016/j.icheatmasstransfer.2010.01.015.

[82] K. Boomsma, D. Poulikakos, On the effective thermal conductivity of a three- dimensionally structured fluid-saturated metal foam, Heat and Mass Transfer **44** (2001) 827–836. doi:http://dx.doi.org/10.1016/S0017-9310(00)00123-X.

[83] M. Pajak, S. Buchaniec, S. Kimijima, J. S. Szmyd, G. Brus, A multiobjective optimization of a catalyst distribution in a methane/steam reforming reactor using a genetic algorithm, International Journal of Hydrogen Energy 46 (2021) 20183–20197. doi:10.1016/j.ijhydene.2020.02.228.

References